Cell Tree Age as a new evolutionary model for representing age-associated somatic mutation burden

Attila Csordas

Ph.D. Thesis

Szeged
2024

Cell Tree Age as a new evolutionary model for representing age-associated somatic mutation burden

Attila Csordas

Ph.D. Thesis

Appointed Consultant: Prof. Dr. Lajos Kemény

University of Szeged
Faculty of Medicine
Doctoral School of Clinical Medicine
Szeged
2024

LIST OF PUBLICATIONS

Scientific papers included in this thesis

I. **Csordas A**, Sipos B, Kurucova T, Volfova A, Zamola F, Tichy B, Hicks DG. Cell Tree Rings: the structure of somatic evolution as a human aging timer. *Geroscience*. 2024 Jan 4. doi: 10.1007/s11357-023-01053-4. Epub ahead of print. PMID: 38172489. **Q1 with IF:5.7**

II. **Csordas A**, Cell lineage trees: the central structure plus key dynamics of biological aging and formulating the limiting problem of comprehensive organismal rejuvenation. *PeerJ Preprints* (2019). **Perspective, not peer reviewed. https://peerj.com/preprints/27821v7/**

Publications not directly related to the thesis

I. Szatmári EZ, **Csordás A**, Kerepesi C. Unique Patterns in Amino Acid Sequences of Aging-Related Proteins. Adv Biol (Weinh). 2023 Oct 25:e2300436. doi: 10.1002/adbi.202300436. Epub ahead of print. PMID: 37880927.

II. Vizcaíno JA, Deutsch EW, Wang R, **Csordas A**, Reisinger F, Ríos D, Dianes JA, Sun Z, Farrah T, Bandeira N, Binz PA, Xenarios I, Eisenacher M, Mayer G, Gatto L, Campos A, Chalkley RJ, Kraus HJ, Albar JP, Martinez-Bartolomé S, Apweiler R, Omenn GS, Martens L, Jones AR, Hermjakob H. ProteomeXchange provides globally coordinated proteomics data submission and dissemination. Nat Biotechnol. 2014 Mar;32(3):223-6. doi: 10.1038/nbt.2839. PMID: 24727771; PMCID: PMC3986813.

III. **Csordas A**, Ovelleiro D, Wang R, Foster JM, Ríos D, Vizcaíno JA, Hermjakob H. PRIDE: quality control in a proteomics data repository. Database (Oxford). 2012 Mar 20;2012:bas004. doi: 10.1093/database/bas004. PMID: 22434838; PMCID: PMC3308160.

IV. Budovsky A, Craig T, Wang J, Tacutu R, **Csordas A**, Lourenço J, Fraifeld VE, de Magalhães JP. LongevityMap: a database of human genetic variants associated with longevity. Trends Genet. 2013 Oct;29(10):559-60. doi: 10.1016/j.tig.2013.08.003. Epub 2013 Aug 30. PMID: 23998809.

V. **Csordás A**. Mitochondrial transfer between eukaryotic animal cells and its physiologic role. Rejuvenation Res. 2006 Winter;9(4):450-4. doi: 10.1089/rej.2006.9.450. PMID: 17105385.

LIST OF ABBREVIATIONS

CTR: Cell Tree Rings

HLC: Healthy Longevity Clinic

MAE: mean absolute error

MdAE: median absolute error

RMSE: root-mean-squared error

scRNA-seq: single-cell RNA sequencing

SNV: single-nucleotide variant

UPGMA: unweighted pair group method with arithmetic mean

Summary

Biological age is typically estimated using biomarkers whose states have been observed to correlate with chronological age. A persistent limitation of such aging clocks is that it is difficult to establish how the biomarker states are related to the mechanisms of aging. Somatic mutations could potentially form the basis for a more fundamental aging clock since the mutations are both markers and drivers of aging and have a natural timescale. Cell lineage trees inferred from these mutations reflect the somatic evolutionary process and thus, it has been conjectured, the aging status of the body. Such a timer has been impractical thus far, however, because detection of somatic variants in single cells presents a significant technological challenge.

Here we show that somatic mutations detected using single-cell RNA sequencing (scRNA-seq) from thousands of cells can be used to construct a cell lineage tree whose structure correlates with chronological age. De novo single-nucleotide variants (SNVs) are detected in human peripheral blood mononuclear cells using a modified protocol. A default model based on penalized multiple regression of chronological age on 31 metrics characterizing the phylogenetic tree gives a Pearson correlation of 0.81 and a median absolute error of ~4 years between predicted and chronological age. Testing of the model on a public scRNA-seq dataset yields a Pearson correlation of 0.85. In addition, cell tree age predictions are found to be better predictors of certain clinical biomarkers than chronological age alone, for instance glucose, albumin levels and leukocyte count.

The geometry of the cell lineage tree records the structure of somatic evolution in the individual and represents a new modality of aging timer. In addition to providing a numerical estimate of ‘Cell Tree Age’, it unveils a temporal history of the aging process, revealing how clonal structure evolves over life span. Cell Tree Rings complements existing aging clocks and may help reduce the current uncertainty in the assessment of geroprotective trials.

Encoding accumulating somatic mutation burden in humans via evolutionary Cell Trees and representing the overall snapshot somatic mutation burden numerically as a Cell Tree Age provides a new model to summarize the most fundamental hallmark of aging, using perhaps the most well established quantitative methodology in biology, phylogenetics.

Introduction

Charles Darwin in the Origin of Species famously used only one diagram, that of an abstract evolutionary tree depicting the hypothetical relations between different species spanning through thousands of generations [Darwin, 2006, p524]. He used this figure to illustrate how the ‘divergence of character’ principle, combined with the principle of ‘natural selection’ ‘tends to act’ on the ‘great Tree of Life’ [Darwin, 2006, p533]. Indeed, a core assumption of any kind of evolutionary theory, independently of any other assumption on mechanisms like natural selection, is that there’s a unified evolutionary tree showing the temporally unfolding branching ancestry of all life on Earth coming from the same ancestor, at the root of the tree.

Since then, phylogenetics and population genetics methods provided biology’s unique, quantitative and at times, predictive toolkit within the natural sciences and have been validated many times over in different applications.

Phylogenetic trees are available in many different flavours depending on the question formulated, operational taxonomic units (OTUs) used at the tips of the tree and the underlying assumptions of the populations modelled. These trees are constructed based on similarities and differences in the genetic and phenotypical characteristics of the biological entities investigated. They can be species trees, answering temporal questions about species divergence, for instance the Tree of Life project tries to place all eukaryotic species on the same phylogenetic tree. Another big variant are gene trees, showing the histories of genetic changes within a particular gene, e.g. haemoglobin, throughout different species and populations. Phylogenomic trees can be species trees built not from particular smaller scale gene, but complex whole-genome data. Trees can be used to track organellar evolution based on specific organellar DNA content in case of mitochondria or chloroplast. Phylogenetic trees are widely used in epidemiology, for instance during the COVID-19 pandemic, the different strains were tracked based on rapidly evolving genetic changes in the spike protein or other regions.

If the leaves on the phylogenetic tree are individual cells that are clonally related and can be traced back through a founder cell through repeated cell divisions, we are talking about a cell lineage tree. The first complete and essentially invariant cell lineage tree of an animal representing 969 cells belonged to C. elegans and was delivered through watching and counting all relevant events (divisions) and cells with light microscopy [Sulston and Horvitz, 1977].

The work using individual genetic differences between cells to reconstruct normal and variant cell lineage trees of the same eukaryotic organism has been started in 2005-06 by two groups, one in Weizmann Institute of Science at Rehovot, in Israel and another in University of

Washington, Seattle, in the USA. First, theoretical results have been delivered to show that based on known microsatellite mutation rates cell lineage trees can be confidently reconstructed from sampling leave cells in trees with mitotic depth of less than 40 divisions. The results have been used in human cell lines to reconstruct cell trees based on microsatellite instability using neighbour-joining algorithm [Frumkin *et al*, 2005]. Second, polyguanine repeat DNA sequences have been used in cultured mouse NIH 3T3 cells to reconstruct cell trees with the help of both Bayesian and neighbour-joining algorithms [Salipante and Horwitz, 2006]. The method was explicitly called phylogenetic fate mapping based on methods used, borrowed from phylogenetics. The breakthrough in vivo result has relied on bulk sequencing 25 organoid cell lines of clonal, endodermal origin extracted from two old mice using 35 somatic base substitutions to reconstruct the cell lineage tree structures with maximum parsimony method [Behjati *et al*, 2014].

Meanwhile, a separate branch of research focused on dissecting intra-tumour heterogeneity, using bulk sequencing methods, and delivering mutational signatures. Most of these tumour phylogenies are not strict cell lineage trees though [Alves *et al*, 2017] as the tips on the trees represent bigger and less well defined entities, than an individual cell.

Earlier studies using data from healthy organisms have naturally focused on developmental biology questions, presenting the cell trees and its properties in a much better understood context than aging.

Aging refers to the systematic decline in cellular and organismal function over time. The ubiquity of age-related disease makes chronological age the single most important risk factor for morbidity and mortality [Partridge *et al*, 2018]. Interventions to slow, delay or even reverse the aging process thus have the potential to mitigate multiple age-related pathologies [Kaeberlein, 2017].

To quantify the effectiveness of such interventions it is necessary to have a reliable measure of biological age. Aging timers, or clocks, accomplish this by using specific biomarkers whose states change systematically with chronological age. A variety of biomarker modalities have been studied, particularly epigenetic, but also transcriptomic, proteomic and metabolomic, among others [Rutledge and Wyss-Coray, 2022, Macdonald-Dunlop *et al*, 2022]. A necessary step in the development of current aging clocks is to show that the chosen biomarker states are associated with chronological age across a population. This correlation captures the average changes over lifespan and establishes a baseline to which individuals can be compared. A desirable property of these biomarker timers is that they be directly linked to the hallmarks of aging [López-Otín *et al*, 2023]. This potentially allows the biomarker states to be interpreted in terms of the mechanisms of aging.

Genome instability due to somatic mutations is the first hallmark of aging [López-Otín *et al*, 2023]. In blood, mutations can lead to somatic mosaicism and eventually clonal haematopoiesis, where cell populations harbouring particular allele variants outgrow others. Animal models of clonal haematopoiesis have been shown to contribute to disease progression [Evans and Walsh, 2023]. More generally, diseases characterized by accelerated aging typically involve the increased accumulation of DNA damage [Lodato *et al*, 2018]. The idea that somatic mutations can drive clonal expansion has stimulated renewed interest in the mutational theory of aging. This represents a new mechanism by which mutations can lead to aging phenotypes [Vijg and Dong, 2020, Massaar and Sanders, 2023] and is distinct from earlier proposals which treated absolute mutation burden as a sufficient cause for organismal aging [Szilard, 1959]. Given its importance as a driver of aging, it would seem that somatic evolution could form the basis for a new type of aging timer.

Somatic mutations (single-nucleotide variants, SNVs, and copy-number variants, CNVs) are naturally occurring barcodes [Sankaran *et al*, 2022] that enable phylogenetic inference of cell lineage trees (cell trees from now on). Cell trees are a representation of the mitotic branching order and clonal structure of a sampled cell population [Salipante and Horwitz, 2006, Wasserstrom *et al*, 2008]. These partial cell trees are subtrees of the whole organismal cell lineage tree which in an adult human consists of tens of trillions of cells [Sender *et al*, 2016]. The shape of a tree refers to the ordering and length of its branches and reflects the clonal structure and evolutionary distances between cells.

Research objectives

The central conjecture behind our proposed aging timer is that the structure, or "shape", of cell trees is a representation of the biological aging process [Csordas, 2019, https://doi.org/10.7287/peerj.preprints.27821v7]. There are two reasons for this hypothesis. The first is that phylogenetic systematics has long shown how genetic distances between species existing today reflect evolutionary changes in the past. It is reasonable then to expect that genetic distances between single cells can be used to infer the somatic evolutionary history of cells, a driver and indicator of aging. The second is that biomedical life history can leave its imprint on the cell tree [Stadler *et al*, 2021], providing a record of major transitions in the aging process. An additional benefit of cell trees is that they provide an intuitively appealing representation of the dynamics of aging that naturally lends itself to interpretation.

Using human peripheral blood cells from healthy individuals (n=18, age range 21-82 years of age) we have developed a new aging timer called Cell Tree Rings (CTR) with the following characteristics:

1. Naturally occurring somatic single nucleotide variants (SNVs) are used to build cell trees using standard phylogenetic algorithms,
2. SNVs are called directly and de novo from scRNA-seq data from hundreds or thousands of cells,
3. A broad set of tree metrics is used to identify aspects of tree shape that are associated with chronological age using a penalized multiple regression model,
4. The model is used to predict a Cell Tree Age for individuals.

Two different types of phylogenetic algorithms, UPGMA and maximum likelihood, are shown to produce a working Cell Tree Age model, providing extra evidence for the hypothesis. Importantly, the model is validated with public data as an independent test set. The predicted Cell Tree Ages are also shown to correlate with some clinical blood biomarkers, for instance glucose, albumin, leukocytes, and monocytes.

Methods

Experimental data and protocol

Biological sample collection and isolation of cells: 18 blood samples, 5 ml each, have been collected by venipuncture at the Healthy Longevity Clinic (HLC) in Prague, Czech Republic. The samples have been taken with informed consent from healthy patients of the clinic. The Healthy Longevity Clinic Ethical Committee has reviewed and approved the Tree Ring Pilot observational study protocol with the reference number 20220301_001. The age range of the volunteers was 21-82 years old at the time of blood collection, 10 volunteers were males and 8 were females. Samples were processed by the same protocol. In the following the data related to the first 6 samples are detailed. Viable peripheral blood mononuclear cells (PBMCs) were isolated from the collected biological sample. 4 ml of peripheral blood was diluted with 4 ml of 2% Fetal bovine serum (FBS) in Phosphate buffered saline (PBS). Subsequently, 8 ml of diluted peripheral blood was carefully layered on top of 4 ml of a density gradient (such as

Lymphoprep^{TM}) and centrifuged at 300 g for 30 min. The cells were carefully harvested from the interface with a plastic pasteur pipette. Then, another 6 ml of 2% FBS/PBS was added to the cells and centrifuged at 300 g for 8 min discarding the supernatant and resuspending the cells in 1 ml of lysis solution. After one-minute incubation on ice, 4 ml of 2% FBS/PBS was added to the cells and centrifuged at 300g for 5 min discarding the supernatant and resuspending the cells in 1 ml of 2% FBS/PBS. Subsequently, the vitality and concentration of cells was determined through Acridine Orange and Propidium Iodide assay at LUNA Automated Cell Counter. Cell concentration range was between 3.72x10^{6} – 6.35x10^{6} b/ml, and cell viability was between 99.1-99.7%.

Labeling the cells with CellPlex: The cells were labelled with molecular tags or CellPlex (according to original protocol CG000391 Cell Labeling with Cell Multiplexing Oligo RevA). Later, a specific volume of each sample was transferred into new 2 ml tubes, and, after labeling, the cells were washed 3 times with 2% FBS/PBS (compared to 2 times in the original protocol). After the last wash, the cells were resuspended in 600 µl of 2% FBS/PBS and counted at LUNA. Cell concentration range was between 3.15x10^{6} – 3.95x10^{6} b/ml, and cell viability was between 99.3-99.7%, post labeling.

The samples were pooled proportionally, and the final pool was passed through a 30 µm filter. Finally, the cells were counted and diluted to optimal concentration.

Loading and library preparation: Cells were loaded on the Chromium Controller and libraries prepared according to the original protocol CG000390 Chromium Next GEM Single Cell3 v3.1 Cell Surface Protein Cell Multiplexing RevB, aiming for 16000 recovered cells. Some library preparation steps were modified slightly. During cDNA amplification, the polymerization step was extended to 1.5 min. After cDNA purification, the samples were split into two aliquots (A and B) that were processed in parallel and differed only in the implementation of size selection. After fragmentation, double size selection was modified for samples according to Table 1 below.

Step	Sample	Volume of 1. SPRI [µl]	Transfer volume [µl]	Volume of 2. SPRI [µl]
After fragmentation	A	20 (0.4x)	65	15 (0.7x)
	B	25 (0.5x)	70	5 (0.6x)
After PCR	A	50 (0.5x)	140	10 (0.6x)
	B	50 (0.5x)	140	10 (0.6x)

Table 1. Double-sided size selection using SPRIselect beads

After PCR amplification, both samples were purified using SPRIselect beads according to Table 1. Finally, the quality and quantity of libraries was determined using the Fragment Analyzer and QuantiFluor dsDNA System.

The various chemicals or kits used were Next GEM Chip G Single Cell Kit, Next GEM Single Cell 3' Gel Beads Kit v3.1, Next GEM Single Cell 3' GEM Kit v3.1, Dynabeads MyOne Silane, Next GEM Single Cell 3' Library Kit v3.1, Single Index Kit T Set A, 3' CellPlex Kit Set A, 3' Feature Barcode Kit, and Dual Index Kit NN SetA.

Sequencing: Library pools were sequenced on an Illumina NovaSeq 6000 using the S4 300-cycle kit and with 150 bp long R2.

Bioinformatics Processing of the experimental data

The output sequencing files have been processed with Cell Ranger v6.0.2 and the indexed paired end bam files have been converted into fastq files with bamtofastq v2.30.0. The fastq files and the identified barcode list were used for further processing.

General schematics of the Cell Tree Rings computational workflow

The Cell Tree Rings computational pipeline involves four consecutive steps, names of the sub-pipelines highlighted in bold.

1. **Tizkit**: Barcode specific calling of SNVs with scSNV and germline filtering.
2. **Tiznit**: Generating fasta files and phylogenetic inference of cell trees.
3. **AgeTreeShape:** Compute tree features and univariate regression on age.
4. **CellTreeAge:** Building multiple penalised regression model and Cell Tree Age prediction.

The following four sections provide further details of this workflow.

Somatic mutation calling de novo from scRNA-seq

We have used scSNV v1.0b [Wilson *et al*, 2021] to call somatic mutations, specifically single nucleotide variants, directly from 10x Genomics scRNA-seq data through collapsed molecular duplicates to increase mutation coverage. The GRCh38 (hg38) reference human genome build was used for mapping and alignment, specifically GENCODE Release 44, GRCh38.p14. Potential germline variants over 1% of minor allele frequency have been removed using the latest version 110 release of the 1000GENOMES vcf file using the Ensembl ftp directory. The 'V3' parameter was set to process 3-prime libraries. The default setting of scSNV has been used with Maximum Variant Allele Fraction set to 0.999. To reduce the number of false positive calls two important consecutive filters were introduced. First, only somatic variants detected by at least 8 different UMIs per barcode have been used, and second, only somatic variants that were present in at least 4 barcodes were considered further for phylogenetic tree generation. The inputs were fastq files and the outputs were sparse SNV count matrices for alternative and reference alleles along with annotated SNV files in csv and vcf format.

Phylogenetic Tree Inference

The matrices and csv files generated in the previous step are used to generate fasta alignments. Fasta files are generated from all the cells and a subset of the cells with SeqKit v2.1.0 [Shen *et al*, 2016]. To track within-sample variability of the trees we generate 5 replicate trees from each sample with each tree being constructed from a random selection of 700 out of the ~1400 cells from that sample. Because these subsets of 700 cells are partially overlapping with each other, each tree is a pseudo-replicate. We will refer to a pseudo-replicate tree as a "partial tree" For phylogenetic inference with UPGMA, the R package phangorn v2.8.1 [Schliep, 2011] was used with helper functions from the ape package v5.6.2. We used the p-distance (the proportion of sites that differ between a sequence pair) to determine branch lengths by setting the evolutionary substitution model to 'raw'. The matrix of pairwise distances was computed with the dist.dna function of the ape package. Tree inference provided rooted, ultrametric trees by default. The trees were stored in newick files.

For Maximum Likelihood, IQ-TREE multicore version 2.2.0-beta COVID-edition was used. The substitution model was JC69.

Cell Trees have been visualised with version 1.4.4 of the FigTree tree figure drawing tool.

Regression Analysis

Elastic net regression

To build a predictor model we regress chronological age on 31 tree statistics in addition to Sex, giving a total of 32 features. We allow pairwise interactions between Sex and each tree statistic giving a total of 32+31=63 predictors.

In line with the majority of previous aging timers [Hannum *et al*, 2013, Horvath, 2013, Levine *et al*, 2018, Rutledge and Wyss-Coray, 2022] we employ elastic net regularization [Zou and Hastie, 2005, Hastie *et al*, 2015]. This requires solving

$$\mu, \hat{\boldsymbol{\beta}} = \arg \min_{(\mu,\boldsymbol{\beta})} \left\{ \frac{1}{2N_{\text{tot}}} \sum_{i=1}^{N_s} \sum_{j=1}^{n_i} \left(y_{ij} - \mu - \boldsymbol{x}_{ij}^{\top} \boldsymbol{\beta} \right)^2 + \lambda \left[\frac{1}{2}(1-\alpha)\|\boldsymbol{\beta}\|_2^2 + \alpha\|\boldsymbol{\beta}\|_1 \right] \right\}, \quad (1)$$

which is a convex program when the hyperparameters λ (the regularization constant) and α (the lasso fraction) are fixed. Here x_{ij} is a predictor and y_{ij} is the chronological age for pseudo-replicate *j* in sample *i*. $\boldsymbol{\beta}$ is the vector of regression coefficients, μ is the constant offset, N_S is the number of samples, n_i is the number of replicates in sample *i* and $N_{\text{tot}} = \sum_{i=1}^{N_s} n_i$ is the total number of replicates across all samples.

Eq. 1 is solved using the elastic-net routine from scikit-learn [Pedregosa *et al*, 20111] (version 1.3.0) in Python3 [Van Rossum and Drake, 2009] (version 3.11.5).

Nested cross validation: To test predictive accuracy using this model we implement a nested cross validation scheme [Varma and Simon, 2006, Cawley and Talbot, 2010]. We used leave-one-out cross-validation in both outer and inner loops: since there are 18 samples this means there were 18 folds in the outer loop and 17 folds in the inner loop (a fold partitions data into a training and test set with each sample assigned to a test set exactly once). All pseudo-replicates from a sample are assigned the same chronological age and are never split across training and test sets.

Hyperparameter grid search: Hyperparameters are determined by solving Eq. 1 multiple times, each time with different hyperparameter value combinations. Hyperparameter values are chosen from the sets $\lambda \in \{0.1,0.3,1,3,10\}$ and $\alpha \in \{0.6,0.7,0.8,0.9,1\}$ in an exhaustive grid search. The hyperparameter combination giving the lowest mean absolute error, as found by cross validation in the inner loop, is chosen as optimal. Once the optimal hyperparameters have been found for a given outer training set, Eq. 1 is solved for one step in the outer loop. The procedure is then repeated for other steps in the outer loop, calculating a new set of hyperparameters each time.

Regression coefficients and prediction accuracy: Each step in the outer loop produces a vector of regression coefficient estimates, $\hat{\beta}$, and a subset of test sample predictions, $\hat{y}_{ij}$. Prediction accuracy is calculated from the full set of predicted and chronological age pairs, $\{\hat{y}_{ij}, y_{ij}\}$. Performance metrics used are the mean absolute error (mae), median absolute error (mdae), root-mean-squared error (rmse), and Pearson correlation (*r*) defined as follows:

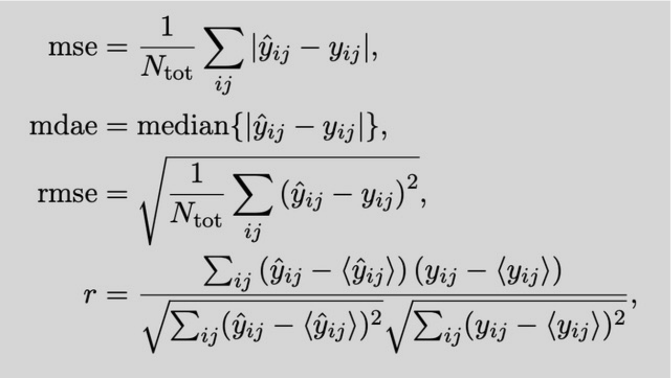

$$
\begin{aligned}
\mathrm{mse} &= \frac{1}{N_{\mathrm{tot}}} \sum_{ij} |\hat{y}_{ij} - y_{ij}|, \\
\mathrm{mdae} &= \mathrm{median}\{|\hat{y}_{ij} - y_{ij}|\}, \\
\mathrm{rmse} &= \sqrt{\frac{1}{N_{\mathrm{tot}}} \sum_{ij} \left(\hat{y}_{ij} - y_{ij}\right)^2}, \\
r &= \frac{\sum_{ij} \left(\hat{y}_{ij} - \langle \hat{y}_{ij} \rangle\right) \left(y_{ij} - \langle y_{ij} \rangle\right)}{\sqrt{\sum_{ij} (\hat{y}_{ij} - \langle \hat{y}_{ij} \rangle)^2} \sqrt{\sum_{ij} (y_{ij} - \langle y_{ij} \rangle)^2}},
\end{aligned}
$$

where, for compactness, we write the double sum $\sum_{i=1}^{N_s} \sum_{j=1}^{n_i}$ as $\sum_{ij}$

This nested cross validation generates a single age prediction for each pseudo-replicate. Because the outer loop has 18 folds, each regression coefficient is estimated 18 times. Results are shown in Figure 2A, 2B.

Testing on public data: A final step in testing the model is to examine its prediction on an external dataset. This involves, in essence, just one step in the outer loop of the nested cross validation where all the 18 HLC samples are used as a single training set, and all the 18 AIDA samples are used as a single test set. Cross validation is still performed in the inner loop to optimize the hyperparameters.

Feature pre-selection

The regularized regression procedure described above combines feature selection and coefficient estimation in a single optimization step. This can result in biased predictions since the regularization required to shrink the weaker predictors also shrinks the better predictors [Hastie *et al*, 2015]. This bias can be mitigated by pre-selecting features in an initial step, prior to elastic net regression [Doherty et al, 2023]. The basic idea is that, by removing some of the weaker predictors prior to regression, the degree of regularization needed in the coefficient estimation step is decreased, thus reducing prediction bias.

Our approach to pre-selecting features is to use the output from the elastic net itself. We take the features selected by the procedure described above and use them in a second (elastic net) regression. This two-step regression approach is similar to adaptive regularization methods where an initial regression step is used to determine feature-specific regularization parameters [Zou, 2006, Zhou and Zang, 2009]. In our scheme, the first regression (the selection step) produces a ranking of features based on the magnitude of their regression coefficients. The second regression (the estimation step) is performed with only the top k ranked features. It is the model fit from this second step that is used for prediction.

To determine the optimal value of k, we repeat the estimation step across different k, finding the value that maximizes performance. Technically, the number of features k is a hyperparameter of the model and should be determined in the inner cross-validation loop, along with α and l_1. This would help account for the uncertainties in post- selection inference [Berk *et al*, 2013 Kammer *et al*, 2022] and reduce the risk of overfitting. However, for our exploratory purposes, we simply perform the estimation step at several different values of k and use the k that gives the best performance.

We find that feature pre-selection does improve predictability, albeit only slightly (see Figure 5). Thus, for simplicity, our default model uses all features, without pre-selection. Nevertheless, demonstrating that a subset of the features provides as good, if not slightly better, predictability as all the features is helpful for reducing the number of regression coefficients that need to be interpreted (see *Discussion*).

Processing Public Datasets

The Asian Immune Diversity Atlas (AIDA) public Human Cell Atlas (HCA) scRNA-seq dataset has been used to process candidate samples for model validation [https://data.humancellatlas.org/explore/projects/f0f89c14-7460-4bab-9d42-22228a91f185]. Fastq files have been downloaded from the HCA site. Filtered barcode lists have been directly downloaded from the CellRanger output available at the Chan Zuckerberg CELLxGENE Collections at the following URL: https://cellxgene.cziscience.com/collections/ced320a1-29f3-47c1-a735-513c7084d508 For scSNV, the 'V2_5P' parameter was set to process the 10X V2 5-prime libraries.

Results

Cell trees

Phylogenetic trees were inferred using the distance matrix algorithm UPGMA and maximum likelihood. To characterise the variability in trees sampled from a single individual in the HLC dataset, we construct trees from 5 subsets of 700 randomly sampled cells rather than a single tree from all ~1400 cells per individual. Because the sets of 700 cells are partially overlapping, we refer to these "partial" trees as pseudo-replicates. Each partial tree is generated using the same filters as described in *Somatic mutation calling de novo from scRNA-seq* in the Methods section. The regression model fit to the HLC dataset is tested on samples from the AIDA dataset using 5 pseudo-replicate trees, each generated from 700 cells per individual.

For visualisation, Figure 1 shows the complete trees utilising information from all ~1400 barcoded cells from each individual in the HLC cohort. The circular rendering, which places the root at the centre and the cells around the perimeter, provided inspiration for the name `Cell Tree Rings'.

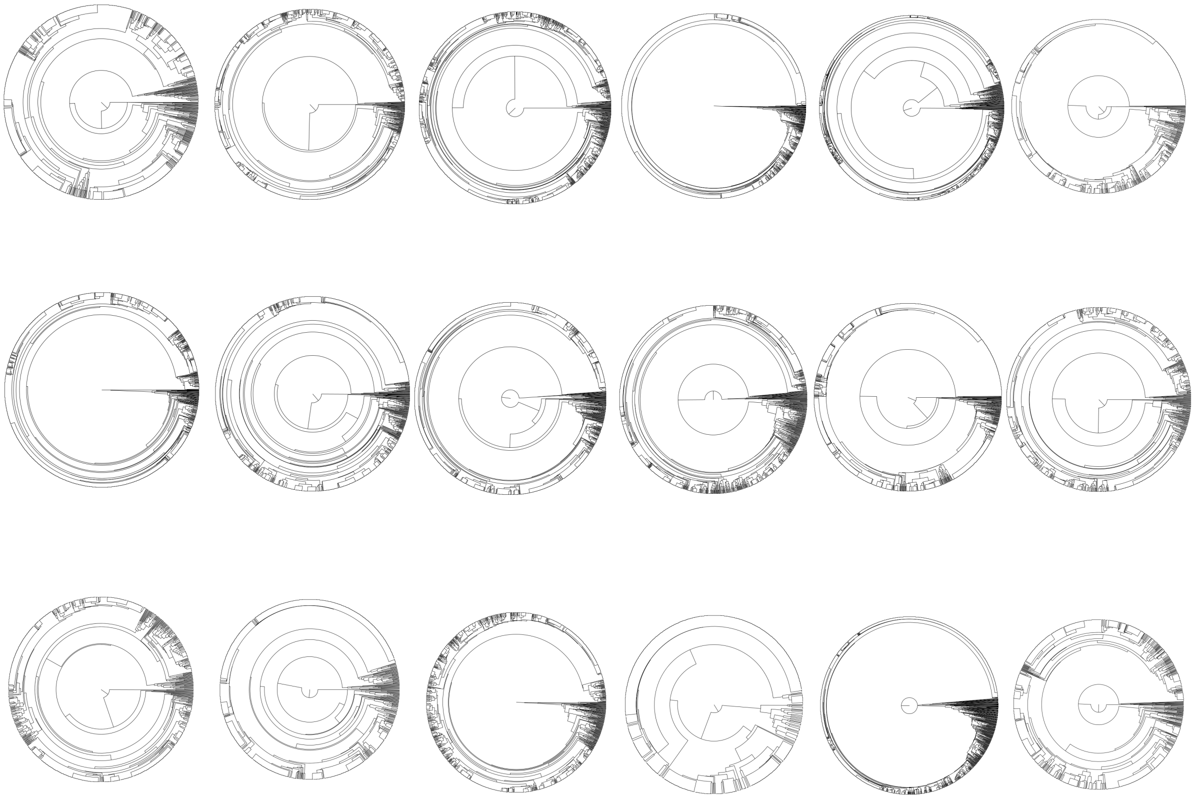

Figure 1: Complete cell trees from each of the 18 HLC participants in the study.

Cell tree metrics

The central hypothesis of the study is that the shape of cell trees is a measure of biological age. Here shape refers to the combination of topology (branching order) and branch lengths. Topology, in the case of cell lineage trees, corresponds to branching patterns of mitotic division in somatic cells. Branch lengths represent the amount of evolutionary change and are usually defined as the product of mutation rates and a suitable unit of time.

Different tree metrics capture either topology-only, branch-length-only, or a combination of both. We have applied a set of 31 tree metrics to characterize the shape of cell trees built from somatic mutations from human peripheral blood mononuclear cells. This set of measures comprises both traditional tree metrics used in phylogenetics and some that were developed specifically for this study.

The tree metrics, or features, can be split into 5 groups based on their technical properties. Group I contains spectral tree metrics that are based on the transform matrices of the cell trees which are discrete analogues of the generalized Fourier [Hicks *et al*, 2019] and Laplacian transforms [20], respectively. Group II contains specialised phylogenetic features focusing on aggregated branch length statistics and their derivatives, including entropy-based metrics. Group III includes well-known general phylogenetic tree statistics used in the biodiversity literature. Group IV focuses on branch length values specifically and generates summary statistics based on the distance matrix between the tips of the tree. Finally, Group V has 2 powergraph based features generating the Laplacian transforms of the square of the tree graphs, similar to Group I.

Group I. Spectral tree metrics

These features implement wavelet [Hicks *et al*, 2019] or spectral graph [Lewitus and Morlon, 2016] analysis of tree shape. In wavelet analysis, the tree is regarded as a signal on the domain of a complete tree and analysed using Haar wavelets. In spectral graph analysis, the eigenvalues of the graph Laplacian are calculated.

I/a. Wavelet-based features

In [Hicks *et al*, 2019] a generalized Fourier transform for functions on a complete tree was derived from symmetry requirements and found to be related to the Haar wavelet basis. Here we apply this transform to the structure of the tree itself. We do this by representing the tree on the nodes of a complete tree: if the tree exists at a node of the complete tree the signal is 1; if it is absent the signal is 0. Since the tree is a small subset of the complete tree there are many zeros in the signal. Thus, to save memory, the transformation is performed by summing only the elements in the transform matrix that multiply 1's in the signal.

The result is a spectrum that characterises the strength of bifurcations in the tree as a function of ℓ, the generation in which the bifurcation originates. This spectrum is summarized using the following metrics:

- avgen_10: The sum of coefficients up to ℓ =10.
- avgen_20: The sum of coefficients up to ℓ =20.
- avgen_40: The sum of coefficients up to ℓ =40.
- avgen_60: The sum of coefficients up to ℓ =60.
- avgen_80: The sum of coefficients up to ℓ =80.
- avgen: The sum of all coefficients.
- avgen_half_g_max: The sum of all coefficients normalized by half the depth of the tree.

I/b. Graph Laplacian tree features

Features in this category are based on either the graph Laplacian, which considers the branching order itself but ignores branch lengths, or the modified graph Laplacian [Lewitus and Morlon, 2016], which incorporates branch lengths as well.

Features based on the Graph Laplacian (GL)

Here the tree is represented as a graph with branches treated as edges and the internal nodes and leaves treated as vertices. Following standard convention, the graph Laplacian is calculated from L = D - A, where D is the diagonal degree matrix and A is the adjacency matrix, composed of a 1 if a pair of nodes is adjacent, and a 0 if not. The vector of eigenvalues of the graph Laplacian is called the spectrum [Lewitus and Morlon, 2016]. The spectrum is characterised using several features:

- Algebraic Connectivity: the second smallest eigenvalue of the non-modified GL matrix.
- Wiener index: 0.5 times the sum of the shortest-path distances between each pair of reachable nodes.
- 'hic': the number of eigenvalues less than or equal to 1.0
- 'cso1': the number of eigenvalues greater than 1.0

Features based on the Modified Graph Laplacian (MGL)

Here the tree is represented as a graph where all the internal nodes and external leaves are used as nodes. The graph Laplacian is modified to account for the length of the branches. This is done by giving each term in the adjacency matrix a weighting determined by the distance between the associated node pair. Eigenvalues (except zero) are log-transformed by taking their natural log. Gaussian kernel convolution is used to also produce a continuous Spectral Density Profile (SDP).

The following eight tree features are determined from the resulting MGL spectrum:

Kurtosis: the fourth central moment divided by the square of the variance of the eigenvalues of the MGL.

Tracer: the maximum height of the Spectral Density Profile.

Skewness: the skewness statistics of the Spectral Density Profile calculated from the 3rd moment μ_3 and 2nd moment μ_2 of the distribution of the eigenvalues of the MGL as $\mu_3/\mu_2^{3/2}$.

Tree Imbalance: the product of Kurtosis and Skewness.

Modified Maximum Eigenvalue: the largest eigenvalue of the MGL.

Modified Maximum Eigengap: the largest difference between two consecutive eigenvalues of the MGL.

Modified Algebraic Connectivity (mAC): the second smallest eigenvalue of the MGL.

Mode Value: The most frequent eigenvalue of the spectral density profile.

Group II. Phylogenetic Branch Length Features and derivatives

Branch Length Log Norm

- The sum of all the branch lengths is computed using the ape R package.
- The sum is normalized by the natural logarithm of the number of tips of the tree.

Mean Branch Length

- The sum of all the branch lengths in the tree is computed using the Bio.Phylo python module.
- The mean branch length is computed by dividing the sum of all the branch lengths by the number of all nodes in the tree.

Entropy based features

These are measures of the spread of pairwise distances between nodes on the tree. The nodes involved can be just the tip nodes or they can be both internal and tip nodes.

Entropy Tips: This requires first finding a histogram of all the pairwise distances between tips of the cell lineage tree, placing each into 50 bins. The Shannon entropy is then calculated from the histogram.

Entropy All Nodes: This is the same as Entropy Tips except pairwise distances between all internal and tip nodes are used.

Group III. Traditional Phylogenetic Features

The tree features listed here are standard in the phylogenetics literature.

Colless index: A statistic designed to assess tree symmetry this is a recursive sum of the differences between left and right leaves at every stage of the tree. Does not consider branch lengths.

Sackin index: A statistic designed to assess tree symmetry this is a sum of all the branches between a root and a leaf summed up for all leaves. Does not consider branch lengths.

Cherries: The number of pairs of adjacent tips on a tree.

Total cophenetic index: Sum of the branch lengths of the lowest common ancestors for all pairs of leaves in the tree. Normalised by the number of leaves in the tree.

tipRootPatr: Captures both topology and branch length information. Each tip node is a certain distance from the root. This distance is summed across all tips.

Group IV. Distance Matrix based Branch Length Features

The features in this group were specifically adapted to the cell lineage tree aging application.

tipDistNorm:

- Distances between the tips of the tree are computed using the branch length information with the distTips function from the adephylo package.
- The sum of all the distances between the tips is computed.
- The sum is normalized by the square of the number of tips used to generate the tree.

tipDistLogNorm:

- Distances between the tips of the tree are computed using the branch length information with the distTips function from the adephylo package.
- The sum of all the distances between the tips is computed.
- The sum is normalized by the natural logarithm of the number of tips in the tree.

tipDistSD

- Distances between the tips of the tree are computed using the branch length information with the distTips function from the adephylo package.
- The standard deviance of the distances between the tips is calculated.

Group V. PowerGraph Features

The square of a binary cell lineage tree is a powergraph and is found by defining node v and node u to be adjacent if, in the original tree, u and v are at most two edges away from each other. Once this powergraph has been generated the Graph Laplacian Matrix can be generated as described above. The natural logarithm of the spectrum of eigenvalues of the Graph Laplacian is computed and the algebraic connectivity found from the second smallest eigenvalue. The algebraic connectivity of a powergraph is a well-known feature of graph robustness.

AC_2: This is the algebraic connectivity from the graph Laplacian of the powergraph.

mAC_2: This is the algebraic connectivity from the modified graph Laplacian of the powergraph.

Default model building and prediction results with all tree features

An age predictor has been constructed by regressing chronological age on the 31 tree metrics, along with Sex. Elastic Net regularization and nested leave-one-out cross validation were used to validate and test the model (See *Regression Analysis* in Methods section). The resulting prediction errors, correlation coefficient, p-values and explained variance were estimated by comparing Cell Tree Ages to chronological ages.

Figure 2 shows the performance of the default Cell Tree Age model cross-validated on the 18 samples from the HLC data. In this default model, UPGMA is used for phylogenetic tree inference, 5 pseudo-replicate trees are used per sample, and all 32 features are used in the regression. For this model, r=0.813, p=0.00004, R^2=0.660, MAE=7.625, MdAE=4.396, and RMSE=10.760.

We also modeled the HLC data with a dummy regressor instead of regressing on tree metrics using the elastic net. The dummy error terms were the following: mae=16.471, mdae=15.882, rmse=19.515. The improvement when including the tree metrics as covariates is apparent.

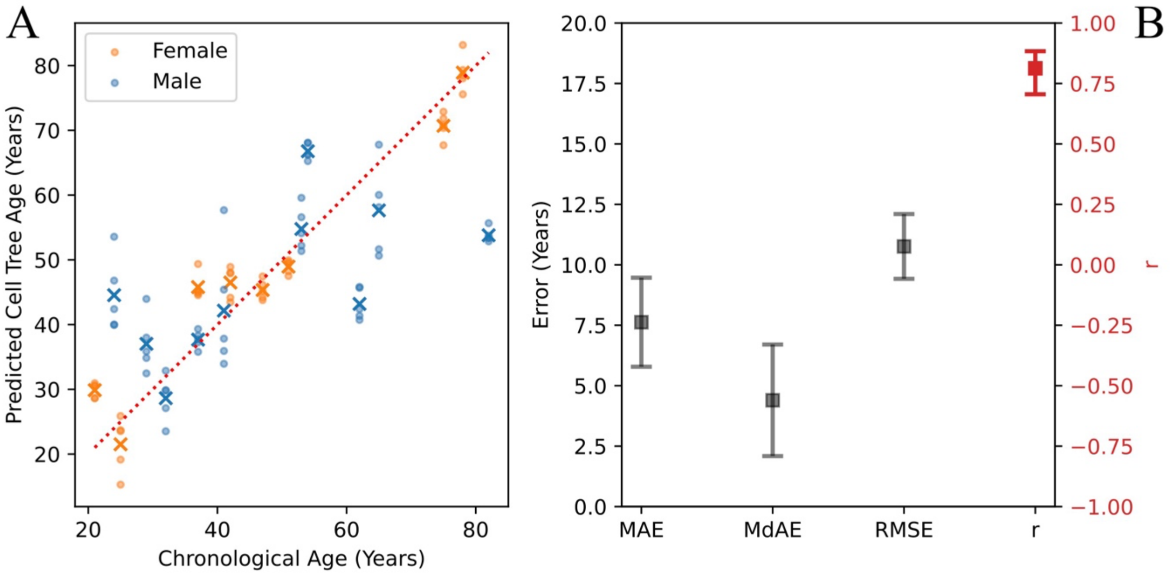

Figure 2: Panel A: Comparison of predicted versus chronological age for 18 human HLC blood samples. Dots represent predictions for each of the 5 pseudo-replicates per sample while crosses represent the mean prediction for each sample. The dotted red line is the reference for perfect prediction (y=x). Panel B: Performance metrics, MAE (mean absolute error), MdAE (median absolute error), RMSE (root mean square error), r (Pearson's Correlation Coefficient).

The slope of predicted to chronological age is less than 1, indicating that low ages are systematically overestimated while high ages are systematically underestimated. This is, in large part, due to regularization which biases the regression coefficients towards zero and thus biases predictions towards the mean of the data. Figure 3A illustrates this trend by showing how the age difference (predicted minus chronological age) is positive below and negative above the mean age of ~47 years. This bias in age prediction can be characterised by a linear trend line (green dashed). It has become customary to refer to the difference between the predicted age and this linear trend line as the "age acceleration" [Horvath, 2013], shown in Figure 3B.

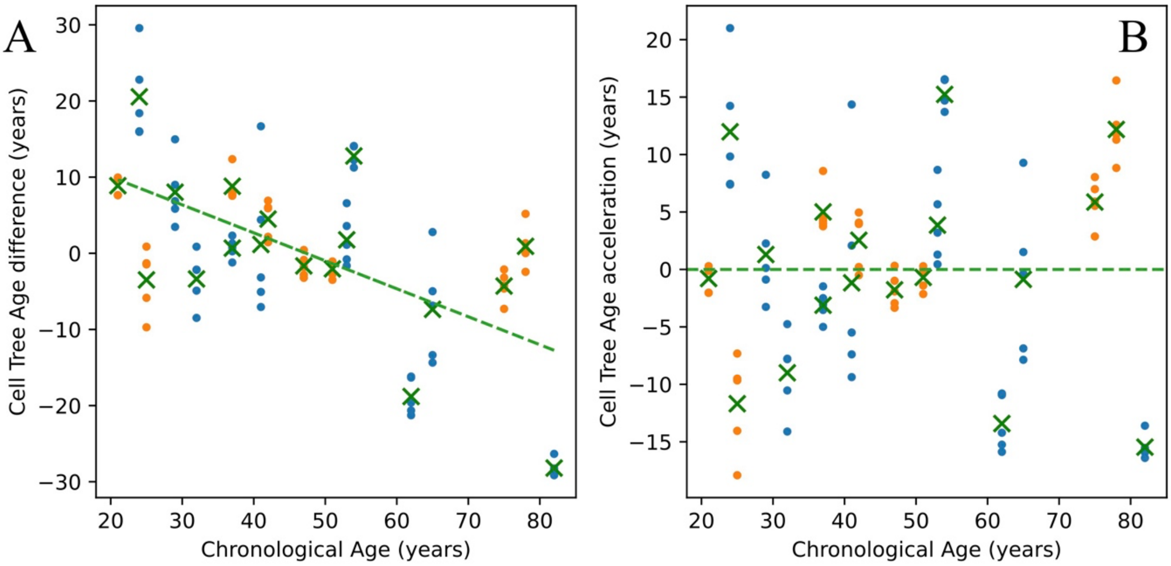

Figure 3: Age difference (Panel A) and age acceleration (Panel B) from the default Cell Tree Age prediction model in Figure 2. The linear trend of predicted to chronological age is given by the green linear. Age difference is predicted age minus chronological age. Age acceleration is the difference between predicted age and the linear fit of predicted to chronological age.

Public Validation of Cell Tree Age Model

Having developed the Cell Tree Age Model on HLC data, we then tested it on a public scRNA-seq dataset. For this we used 18 peripheral blood samples from the Asian Immune Diversity Atlas (AIDA). This involved 10 females and 8 males ranging in age between 21 – 65 years old. For these data, as with the HLC data, we used UPGMA to generate 5 pseudo-replicate trees from each sample where each pseudo-replicate used 700 cells randomly selected from the sample. The default model was trained on all 18 of the HLC data (see *Testing on Public Data* in the *Regression Analysis* section). The resulting performance metrics were *r*=0.853, *p* = 0.00001, R^2=0.728, MAE=12.791, MdAE=13.636, RMSE=14.081.

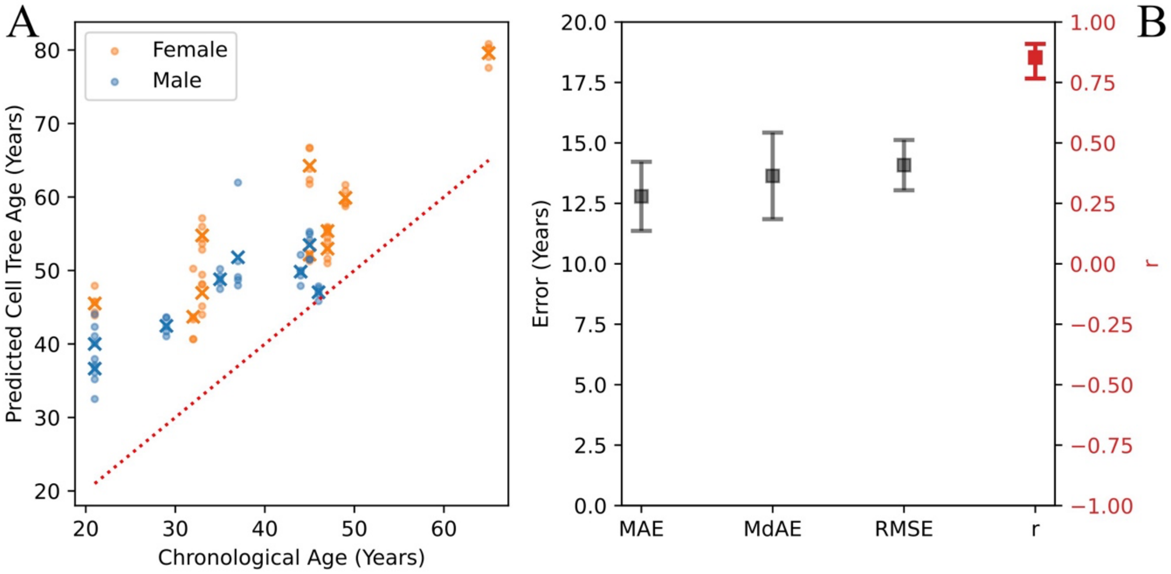

Figure 4: Panel A: Comparison of predicted vs chronological ages for 18 independent human blood samples from the public AIDA dataset. The default model, without feature pre-selection, was trained on 18 samples from the HLC dataset. As in Figure 2, dots represent predictions for each of the 5 pseudo-replicates per sample while crosses represent the mean prediction for each sample. The dotted red line is the reference for perfect prediction (y=x). Panel B: Performance metrics, MAE (mean absolute error), MdAE (median absolute error), RMSE (root mean square error), *r* (Pearson's Correlation Coefficient).

Cell Tree Age model with feature pre-selection using UPGMA

Applying feature pre-selection (*Regression Analysis*) on the HLC training set resulted in the best performing Cell Tree Age model using 5 tree features 'tipDistNorm', 'mMax_eigengap', 'mMaxEigen', 'AC_2', 'tipRootPatr' (see definition in Cell Tree Metrics section above) and interaction terms with 'Sex' binary variable with the smallest errors and highest correlation coefficients: r=0.908, p = 0.000001, R^2=0.825, MAE=5.690, MdAE=3.480, RMSE=7.782. Figures 5A and 5B show how the performance metrics change when using between 1 to 32 of the ranked features. Results from the best performing model, with 6 features, are shown.

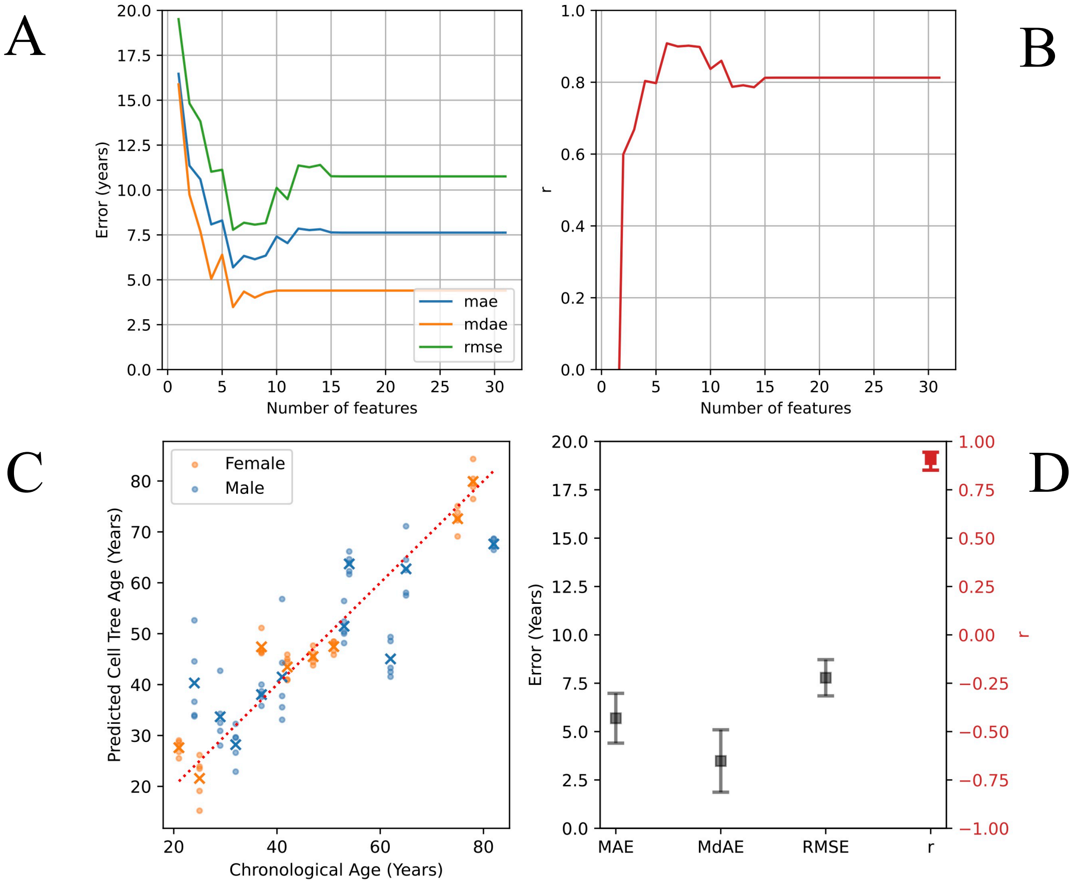

Figure 5: Panel A and B: Performance metrics as a function of the number of the top ranked features used. The most accurate model built using UPGMA trees is the 6-feature model (5 tree metrics and Sex). Panel C and D: Cell Tree Age performance on 18 human HLC blood samples using the 6 feature model selected with feature pre-selection.

Cell Tree Age performance on public data with feature pre-selection using UPGMA

Figure 6 shows performance of the Cell Tree Age model on the 18 AIDA datasets with only 4 tree features selected with ‘Sex’ as interaction term. These 4 tree features are 'tipDistNorm', 'mMax_eigengap', 'mMaxEigen', 'AC_2' and the performance metrics are r=0.721, p = 0.00074, R^2=0.519, MAE=8.942, MdAE=7.548, RMSE=10.894.

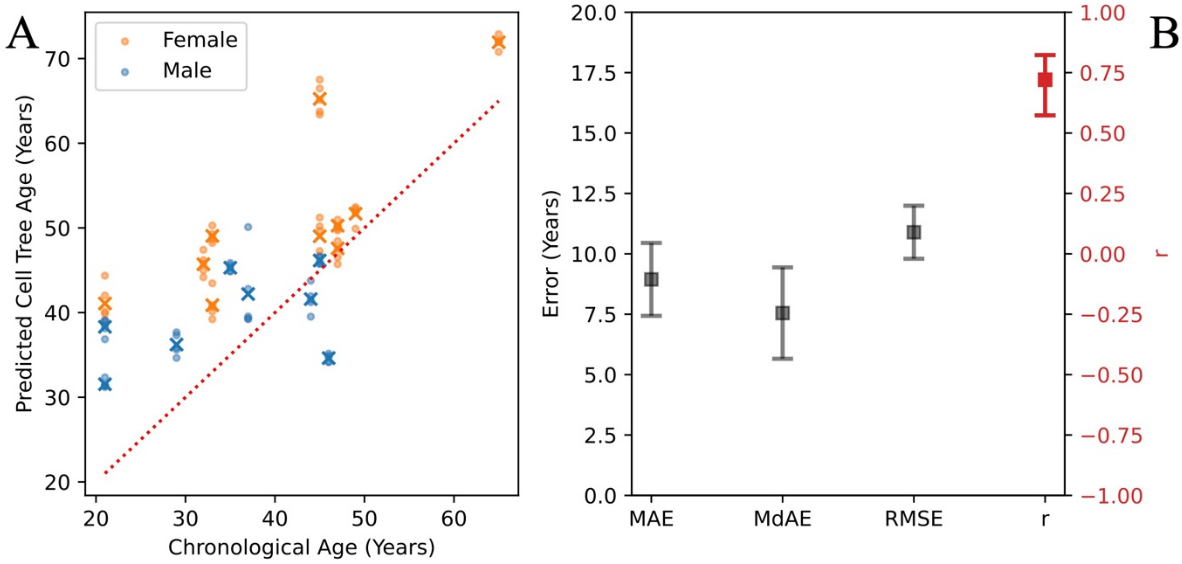

Figure 6: Panel A and B: Performance of the model on the public AIDA dataset, after training on the HLC dataset. Uses feature pre-selection with 4 features plus Sex. Panel B: the statistics of leave-one-out cross validation shows mean performance metrics of the model, MAE, MdAE, RMSE are Mean Absolute Error, Median Absolute Error, Root Mean Squared Error in years, correspondingly, and r is Pearson's Correlation Coefficient.

Cell Tree Age model and feature pre-selection with Maximum Likelihood

For evaluating the Maximum Likelihood tree method, 5 pseudo-replicate trees using 700 randomly sampled cell each were constructed with IQ-TREE. Figure 7 below shows the default all feature model with performance metrics r=0.694, p = 0.00139, R^2 =0.482, MAE=9.701, MdAE=6.060, RMSE=13.424.

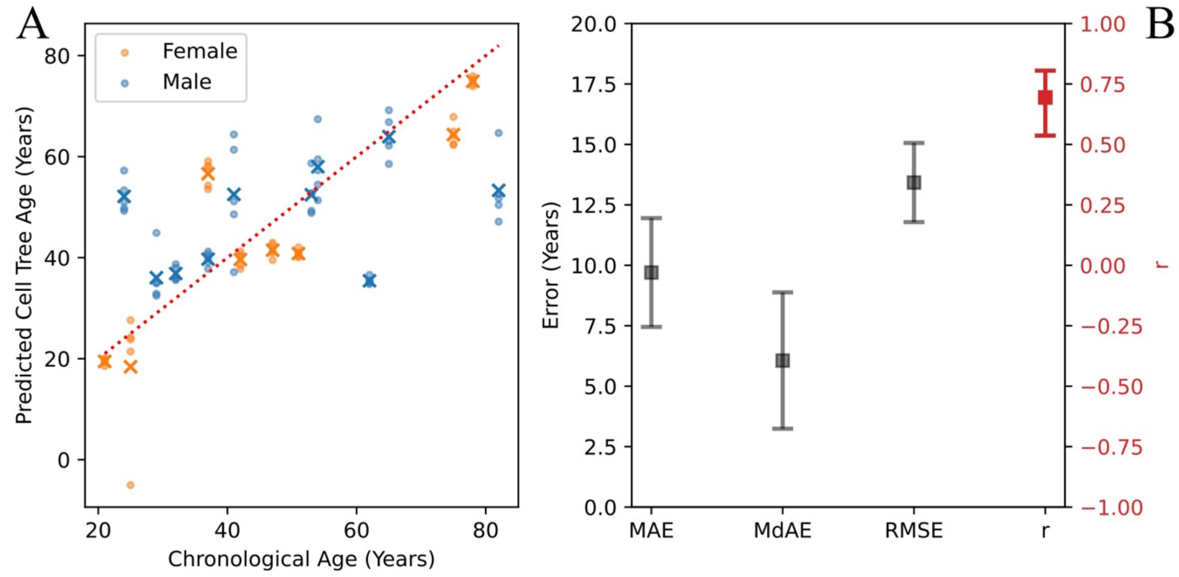

Figure 7: Cell Tree Age prediction performance on the 18 HLC human blood samples based on trees inferred using maximum likelihood (rather than UPGMA). This model uses only three tree features and Sex as an interaction term.

Figure 8 below shows performance metrics of scanning through the number of ranked features with feature pre-selection and the scatter plot and performance metrics of the best performing maximum likelihood-based model with performance metrics 6 features selected with performance metrics r=0.797, p = 0.00007, R^2=0.636, mae=8.260, mdae=5.654, rmse=11.144. The 5 tree features are 'mMaxEigen', 'mMax_eigengap', 'avgen_10', 'avgen', 'tipRootNodes' plus 'Sex', with ‘Sex-only’ interaction terms allowed.

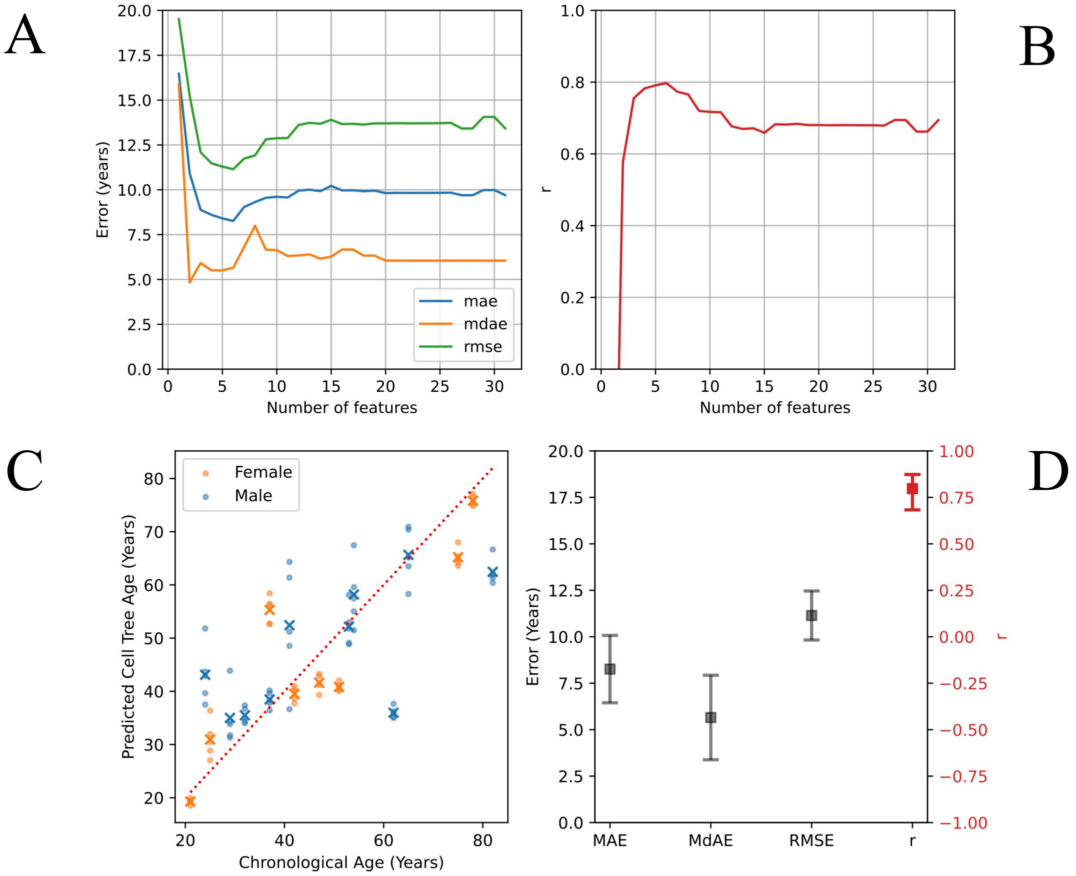

Figure 8: Panel A and B: Feature pre-selection showing performance metric changes when selecting an increasing number of minimum features, error terms on A and correlation coefficient on the right panel. The most accurate model built using Maximum Likelihood trees is a 6 feature model (5 tree metrics and Sex), where mean and root mean squared errors are the smallest and correlation coefficient is the highest. Panel C and D: Performance of the most accurate 6 feature model selected with feature pre-selection.

Cell Tree Age associations with clinical biomarkers

As part of the approved study protocol, a wide range of clinical blood biomarker work has been shared. These were obtained during the same period as the blood draws for the scRNA-seq. For the following list of clinical blood markers, we had access to values of 13 samples out of the 18 HLC samples, 9 males and 4 females: complete leukocyte and erythrocyte blood panel (13 markers), albumin, glucose, hba1c, total cholesterol, alkaline phosphatase, uric acid, creatinine, blood urea nitrogen. This provided a total of 21 markers.

Table 2 shows statistically significant associations between predicted Cell Tree Ages and Chronological Ages and several of the blood markers. The most accurate model was used for the predicted Cell Tree Ages, involving 6 pre-selected features (see Figure 5).

Since reference ranges can differ between females and males for particular blood markers and since we had 9 male samples available compared with 4 female samples, male-specific results are provided as well in order to examine their associations with predicted Cell Tree Age and Chronological Age.

Out of the 21 blood markers, 8 markers were associated significantly with Cell Tree Age or Chronological Age or both. Six out of these 8 significant associations showed Cell Tree Ages to be stronger predictors than Chronological Age with the metabolic marker blood glucose showing the biggest difference.

Clinical marker	Correlation Cell Tree Age as predictor	Correlation Chronological Age as predictor	Group	Unit
Albumin	-0.71*	-0.67*	All	g/L
Albumin	-0.69*	-0.63	Male	g/L
Glucose	0.78*	0.58	All	mmol/L
Hba1c	0.77*	0.73	Male	mmol/mol
Monocytes	0.89*	0.83*	All	10^9/l
Monocytes	0.95*	0.92*	Male	10^9/l
Neutrophils	0.76*	0.72*	Male	10^9/l
Leukocytes	0.61*	0.56	All	10^9/l
Leukocytes	0.83*	0.72*	Male	10^9/l
Mean Red Cell Volume	0.64	0.70*	Male	fL
Lymphocytes	-0.52	-0.63*	All	10^9/l

Table 2. Statistically significant associations between cell tree age and various clinical markers. For comparison, associations between chronological age and same clinical markers are also shown. Asterisks indicate p-value<0.05.

Discussion

We have shown that cell trees constructed using SNVs from human peripheral blood mononuclear cells can predict chronological age. The SNVs underlying these trees can be directly called from the most accessible single-cell sequencing approach, scRNA-seq. Importantly, the trained Cell Tree Age model was validated on an independent test set and the predicted Cell Tree Age was found to be significantly associated with several blood markers (see *Cell Tree Age associations with clinical biomarkers*).

The resulting new molecular aging timer, Cell Tree Rings, requires dozens of cell tree metrics as inputs. Performance of this default model can be improved by ranking the features and regressing on a subset of them (See Feature Pre-Selection in *Regression Analysis* section). Figure 1 shows that pre-selection of between 5-12 features improves predictive accuracy. At peak accuracy, using 6 regressors (Sex, 'tipDistNorm', 'mMax_eigengap', 'mMaxEigen', 'AC_2', 'tipRootPatr') results in predictions with a median absolute error of ~3.5 years, a correlation coefficient of 0.9 and ~82% explained variance. Note that accuracy rapidly declines with fewer predictors such that univariate prediction, even with the single best regressor, has poor accuracy.

Feature selection is useful for identifying the metrics important for prediction. ‘mMax_eigengap’ has been used as a heuristic to identify different modes of divisions or modalities within the tree [Lewitus and Morlon, 2016]. 'AC_2' is the algebraic connectivity of a graph, a well-known feature of graph robustness. Overall, these tree metrics may represent a conceptually new and experimentally verifiable class of quantitative predictors of age.

The Maximum Likelihood method for phylogenetic inference serves as important additional phylogenetic evidence to justify the Cell Tree Age model approach (See Figure 7). On the HLC data the best performing model contained 6 predictors with performance metrics r=0.797, p = 0.00007, mae=8.260, mdae=5.654 (See Figure 8).

Most importantly, the Cell Tree Age model, trained on the HLC data, when tested on samples from the public AIDA dataset gave an *r* of 0.85 indicating that the model does generalize to existing public data. To further the generalizability, the HLC data came from a Central European cohort, the AIDA data were from an East Asian cohort. However, despite this strong correlation between predicted and chronological age, the clock appears to systematically overestimate age in the AIDA data (see Figure 4). Although feature pre-selection reduces this bias (Figure 6), there is still a clear overestimate of age.

There are differences between the HLC training set and the AIDA test set that might account for this batch effect. While the HLC data used 10x V3 3’ prime-end libraries, the AIDA data used 10X V2 5’ prime-end libraries. This means that the former method detects variants in the 3’ end region of the genes, including UTR regions, the latter detects variants from the 5’ prime end region, including regulatory elements. Furthermore, the AIDA dataset is primarily restricted to the 20-50 year old age range, with just a single sample over 60. Further investigations are needed to understand this batch effect.

We believe Cell Tree Rings to be the only existing natural barcoding approach that can build larger trees from thousands of cells using somatic mutations called de novo from scRNA-seq data alone as well as from all autosomes, sex chromosomes and the mitochondrial genome combined. Representative cell trees can capture multiple clonal events in different parts of the accessible cellular genomes, reaching a higher resolution in cell population history than possible with targeted genomics approaches alone.

Another advantage of Cell Tree Rings is its potential to extract both lineage histories and gene expression levels from the same cells using a single method and lab protocol. Combining lineage and phenotypic expression information from the same sample is a considerable challenge and existing approaches offer complex solutions combining different protocols [Lähnemann *et al*, 2020].

We have also examined the association of Cell Tree Age with 21 clinical blood markers (see *Cell Tree Age associations with clinical biomarkers*). Of the 8 markers that show significant associations with Cell Tree or chronological age, 6 of them are better correlated with Cell Tree age than chronological age. These results provide a preliminary indication of how Cell Tree Age could provide valuable clinical indicators. Ultimately, clocks measuring biological age must be better predictors of clinical markers than chronological age. Not all of these associations were related to explicit immune functions, for instance the glucose and albumin associations suggest that if these results are confirmed on bigger cohorts, then Cell Tree Rings might provide a measure of broader multi-tissue and multi-organ age modalities.

Methodological Comparison between single cell DNA and RNA sequencing of somatic mutations

Although single-cell whole-genome DNA sequencing would appear to be the most obvious and comprehensive solution for calling somatic SNVs in single cells there are two main reasons we chose to pursue a scRNA-seq protocol. The first is translational in that we seek to develop a simpler, more affordable platform for clinical application that can be scaled up to meet increasing demand. The second reason is scientific.

In terms of translational arguments, there are 4 different but overlapping aspects of choosing scRNA-seq over single-cell whole-genome DNA sequencing to generate cell lineage trees: affordability, costs, scale, and complexity of protocols.

1. Affordability: Few laboratories have the resources to perform single cell, whole-genome DNA sequencing combined with error-corrected sequencing. Single-cell RNA

sequencing, in contrast, is a commercially available technique now used in hundreds of facilities worldwide.

2. Costs: single cell, whole-genome DNA sequencing costs are an order of magnitude greater than commercially available single-cell RNA sequencing.
3. Scale: Because of these high costs, current cell lineage tree analysis using whole genome scDNA-seq protocols is likely difficult to scale beyond a few hundred cells. In the Mitchell et al. study [Mitchell *et al*, 2022] an average number of 358 cells were studied over 10 individuals. In our first implementation of the Cell Tree Rings method we have already studied an average of 1358 cells over 18 samples. With the external validation set, we have added 18 public samples to the original 18 HLC samples, giving a total of 36 samples. This demonstrates the ability, potentially, to extract hundreds or thousands of new cell trees from existing public scRNA-seq samples with Cell Tree Rings methodology and add it to the model. Also it is straightforward to scale this to tens of thousands of cells or more.
4. Protocol: Our technique can be implemented in essentially any 10x Chromium sequencing facility and the public validation of our data shows that it can be retrospectively applied to datasets already generated worldwide. In contrast, the [Mitchell *et al*, 2022] whole genome scDNA-seq protocol requires growing colonies from the sampled individual cells in vitro and extensive QC steps to control for the artificially introduced genome changes.

In terms of scientific arguments there are 3 aspects to consider currently:

1. Genome Coverage: One obvious advantage of single-cell whole-genome DNA sequencing is the ability to track somatic mutations across the whole genome, while sc-RNA-seq is restricted to protein coding and nearby regulatory regions. However the current study proved that cell lineage trees generated from scRNA-seq data can reliably deliver a strong age signal.
2. Transcriptomics information: Because we are calling variants from RNA transcripts our method has the potential to integrate both genomics and transcriptomics modalities. We anticipate that an scRNA-seq aging timer which has both gene expression and variant information will result in a more versatile and insightful aging timer than an scDNA-seq timer which has variant information alone. However our current study, the first implementation of Cell Tree Rings, has focused on using mutation information alone.
3. Cell type access: Our scRNA-seq based method captures blood cells from a wide variety of myeloid and lymphoid lineages. These can be at different maturity states, from stem

cells to fully differentiated white blood cells. In contrast, scDNA-seq techniques are more restricted to certain cell types. For example, if growing colonies in vitro is required, as in the [Mitchell *et al*, 2022] study, it may only be possible to study hematopoietic stem and progenitor cells, but not more mature phenotypes.

Potential directions for improvement in CTR

The version of CTR reported here represents a basic proof-of-principle. Here we discuss some of the improvements envisioned. The current version of Cell Tree Rings has been achieved with direct and de novo scRNA-seq alone without the aid of any bulk sequencing approach. At a technical level, bulk exome sequencing data can improve true mutation calls at the single cell level and filter out more noise.

In the future, some of this residual variation in predicated age could be explained by individual medical histories or phenotypes, when they become available. In addition, as mentioned above, gene expression information can be extracted from the same cellular barcodes and from the very same genes whose SNVs have been used to generate the cell tree. Efforts are currently underway to see how much of the currently unexplained variation can be accounted for by the cellular phenotypes and the individual medical histories.

Translational geroscience seeks to identify which elements of the aging process are irreversible under current available treatments and which are amenable to modification by existing therapeutic interventions. The tree features involved in Cell Tree Rings may be valuable in diagnosing the influence of a particular intervention by examining its effect on tree shape.

When extending Cell Tree Rings to other tissues an important question is how spatial aspects of the tree can be incorporated. Cellular elements in complex biofluids, such as blood and saliva, have considerable freedom of movement throughout the human body. In contrast, resident cells of compact, solid tissues in the kidney, intestine, liver for instance are under considerable spatial restrictions. The infiltrating immune cells of compact tissues are less constricted spatially than the resident cells, but more constricted than circulating blood cells. It is an open question how tree shape metrics contributing to the age regression model will change in a more restricted spatial environment. Spatial restrictions have been shown to be important in cancer where evolutionary phylodynamic models have been applied to model boundarydriven solid tumor growth [Lewinsohn *et al*, 2023]. Combining spatial information with the temporal information of cell trees could thus help improve the ability of cell trees to quantify biological age.

Questions that Cell Tree Rings can help answer

One surprising finding in the phylogenetic tree-aided developmental biology literature is the degree of asymmetry in phylogenetic lineage trees [Bizzotto *et al*, 2021, Fasching *et al*, 2021]. These studies showed how, at least on the few samples studied, there can be a substantial difference in the number of surviving progeny between offspring of the first or first few cell divisions, the asymmetry reaching sometimes as large as 10:90%. Cell Tree Rings can help quantify this developmental imbalance further and separate it from changes in later life.

Somatic mutations in a small set of (growth and cancer associated) genes have been shown to propagate clones that become dominant in the hematopoietic system of older individuals [Mitchell *et al*, 2022] and have been directly linked to increased risk of cancer and other chronic diseases [Marongiu and DeGregori, 2022]. Additionally, somatic mosaicism has been shown, in multiple tissues, to rise with age and to predict disease in animal models [Evans and Walsh, 2023].

From the perspective of designing interventions, it is important to understand which of the somatic mutations are simply passive indicators and which are active drivers of the aging process. In addition, it will be important to establish which can be targeted with clinical interventions.
By providing a way to quantify the different aspects of tree shape, Cell Tree Rings can be used to identify early indicators of clonal hematopoiesis and diagnose why certain individuals display resilience to the effects of somatic mutation and experience reduced chronic age-associated disease.

Cell Tree Rings and the timescales and convergence of different clocks

When evaluating the effectiveness of different biological aging clocks, it is important to address the question of what the minimal meaningful temporal unit of biological aging is. While clocks with high temporal resolution can evaluate the short-term effects of interventions, these effects can often be difficult to distinguish from physiological noise. On the other hand, lower temporal resolution over longer time windows may miss important short-term signals [Gabbutt *et al*, 2022]. Cell Tree Rings captures the long-term dynamics of somatic evolution that relates to the decades-long processes usually associated with aging but is insensitive to processes that are shorter than the characteristic timescale for detecting somatic mutations. It is an open question whether clocks based on different mechanisms and with different time resolutions can be combined and merged, but ultimately the results from different clocks should be reconciled.

Our hope is that Cell Tree Rings may provide a baseline integrative framework for different aging hallmarks and clocks. There are three reasons this may be possible:

First, Cell Tree Rings operate on the fundamental genome-instability level by tracking somatic mutations in hundreds or thousands of single cells. Importantly, it is the use of the tree structure to constrain these mutations that helps to improve their detection accuracy.

Second, Cell Tree Rings is based on a foundational construct, the somatic evolutionary cell tree, that relates the tens of trillions of somatic cells of a human body to each other and to time.

Third, without identifying the damage somatic mutations cause, it is difficult to design healthy longevity therapies and regimens. Cell Tree Rings captures and organizes this basic mutation information at different levels of the tree hierarchy, potentially providing signposts for which interventions are likely to be most effective.

Cell Tree Rings is thus not simply another aging timer. It aims to provide a foundational principle for clocks. There is considerable uncertainty about whether epigenetic aging clocks can inform us about biological age reversals in clinical trials [Higgins-Chen *et al*, 2022]. Adding Cell Tree Rings as a single-cell resolution clock component might mitigate this uncertainty and improve the assessment of geroprotective trials.

Acknowledgements

I'd like to express my gratitude to **Professor Lajos Kemény** for giving me the opportunity to enroll into the PhD. under special regulation program at Szeged, the city, that has been at the forefront of Hungarian biomedical sciences for so many decades and the place where I, a person born and raised in Budapest, have also obtained my biology MS Degree, and always felt at home.

My biggest acknowledgement goes to my two co-inventors of the Cell Tree Rings method, **Professor Damien G. Hicks,** and **Dr. Botond Sipos**.

Special thanks to our collaborators, **Dr. Boris Tichy** and **Terezia Kurucova**, at the sequencing lab in Brno, at the Central European Institute of Technology, Masaryk University.

We would like to acknowledge the patients of Healthy Longevity Clinic in Prague, who volunteered to provide blood and **Dr. Frantisek Zamola** and **Andrea Volfova** for their help in the recruiting and blood collection procedure.

Special acknowledgement goes to **Petr Sramek**, of LongevityTech.Fund for providing crucial infrastructure in the Czech Republic.

Special thanks to **Dr. Gavin Wilson** for insights on the scSNV pipeline.

References

Alves JM, Prieto T, Posada D. Multiregional Tumor Trees Are Not Phylogenies. Trends Cancer. 2017 Aug;3(8):546-550. doi: 10.1016/j.trecan.2017.06.004.

Behjati S, Huch M, van Boxtel R, Karthaus W, Wedge DC, Tamuri AU, Martincorena I, Petljak M, Alexandrov LB, Gundem G, Tarpey PS, Roerink S, Blokker J, Maddison M, Mudie L, Robinson B, Nik-Zainal S, Campbell P, Goldman N, van de Wetering M, Cuppen E, Clevers H, Stratton MR. Genome sequencing of normal cells reveals developmental lineages and mutational processes. Nature. 2014 Sep 18;513(7518):422-425. doi: 10.1038/nature13448.

Berk, R., Brown, L., Buja, A., Zhang, K., and Zhao, L. (2013). Valid post-selection inference. The Annals of Statistics, 41(2):802 – 837.

Bizzotto S, Dou Y, Ganz J, Doan RN, Kwon M, Bohrson CL, Kim SN, Bae T, Abyzov A; NIMH Brain Somatic Mosaicism Network, Park PJ, Walsh CA. Landmarks of human embryonic development inscribed in somatic mutations. Science. 2021 Mar 19;371(6535):1249-1253. doi: 10.1126/science.abe1544.

Cawley, G. C. and Talbot, N. L. (2010). On over-fitting in model selection and subsequent selection bias in performance evaluation. J. Mach. Learn. Res., 11:2079–2107.

Darwin, C. (2006). From So Simple a Beginning, The Four Great Books of Charles Darwin. W.W. Norton & Company.

Doherty, T., Dempster, E., Hannon, E., Mill, J., Poulton, R., Corcoran, D., Sugden, K., Williams, B., Caspi, A., Moffitt, T. E., Delany, S. J., and Murphy, T. M. (2023). A comparison of feature selection methodologies and learning algorithms in the development of a dna methylation-based telomere length estimator. BMC Bioinformatics, 24(1):178.

Evans MA, Walsh K. Clonal hematopoiesis, somatic mosaicism, and age-associated disease. Physiol Rev. 2023 Jan 1;103(1):649-716. doi: 10.1152/physrev.00004.2022.

Fasching L, Jang Y, Tomasi S, Schreiner J, Tomasini L, Brady MV, Bae T, Sarangi V, Vasmatzis N, Wang Y, Szekely A, Fernandez TV, Leckman JF, Abyzov A, Vaccarino FM. Early developmental asymmetries in cell lineage trees in living individuals. Science. 2021 Mar 19;371(6535):1245-1248. doi: 10.1126/science.abe0981.

Frumkin D, Wasserstrom A, Kaplan S, Feige U, Shapiro E. Genomic variability within an organism exposes its cell lineage tree. PLoS Comput Biol. 2005 Oct;1(5):e50. doi: 10.1371/journal.pcbi.0010050.

Gabbutt C, Schenck RO, Weisenberger DJ, Kimberley C, Berner A, Househam J, Lakatos E, Robertson-Tessi M, Martin I, Patel R, Clark SK, Latchford A, Barnes CP, Leedham SJ, Anderson ARA, Graham TA, Shibata D. Fluctuating methylation clocks for cell lineage tracing at high temporal resolution in human tissues. Nat Biotechnol. 2022 May;40(5):720-730. doi: 10.1038/s41587-021-01109-w.

Hannum, G., Guinney, J., Zhao, L., Zhang, L., Hughes, G., Sadda, S., Klotzle, B., Bibikova, M., Fan, J.-B., Gao, Y., Deconde, R., Chen, M., Rajapakse, I., Friend, S., Ideker, T., and Zhang, K. (2013). Genome-wide methylation profiles reveal quantitative views of human aging rates. Molecular Cell, 49(2):359–367.

Hastie T, Tibshirani R, Wainwright M. Statistical Learning with Sparsity: The Lasso and Generalizations, CRC Press, 2015.

Hicks DG, Speed TP, Yassin M, Russell SM. Maps of variability in cell lineage trees. PLoS Comput Biol. 2019 Feb 12;15(2):e1006745. doi: 10.1371/journal.pcbi.1006745.
Higgins-Chen AT, Thrush KL, Wang Y, Minteer CJ, Kuo PL, Wang M, Niimi P, Sturm G, Lin J, Moore AZ, Bandinelli S, Vinkers CH, Vermetten E, Rutten BPF, Geuze E, Okhuijsen-Pfeifer C, van der Horst MZ, Schreiter S, Gutwinski S, Luykx JJ, Picard M, Ferrucci L, Crimmins EM, Boks MP, Hägg S, Hu-Seliger TT, Levine ME. A computational solution for bolstering reliability of epigenetic clocks: Implications for clinical trials and longitudinal tracking. Nat Aging. 2022 Jul;2(7):644-661. doi: 10.1038/s43587-022-00248-2.

Horvath, S. (2013). DNA methylation age of human tissues and cell types. Genome Biology, 14(10):3156.

Kaeberlein M. Translational geroscience: A new paradigm for 21st century medicine. Transl Med Aging. 2017 Oct;1:1-4. doi: 10.1016/j.tma.2017.09.004.

Kammer, M., Dunkler, D., Michiels, S., and Heinze, G. (2022). Evaluating methods for lasso selective inference in biomedical research: a comparative simulation study. BMC Medical Research Methodology, 22(1):206.

Lähnemann D, Köster J, Szczurek E, McCarthy DJ, Hicks SC, Robinson MD, Vallejos CA, Campbell KR, Beerenwinkel N, Mahfouz A, Pinello L, Skums P, Stamatakis A, Attolini CS, Aparicio S, Baaijens J, Balvert M, Barbanson B, Cappuccio A, Corleone G, Dutilh BE, Florescu M, Guryev V, Holmer R, Jahn K, Lobo TJ, Keizer EM, Khatri I, Kielbasa SM, Korbel JO, Kozlov AM, Kuo TH, Lelieveldt BPF, Mandoiu II, Marioni JC, Marschall T, Mölder F, Niknejad A, Raczkowski L, Reinders M, Ridder J, Saliba AE, Somarakis A, Stegle O, Theis FJ, Yang H, Zelikovsky A, McHardy AC, Raphael BJ, Shah SP, Schönhuth A.

Eleven grand challenges in single-cell data science. Genome Biol. 2020 Feb 7;21(1):31. doi: 10.1186/s13059-020-1926-6.

Levine, M. E., Lu, A. T., Quach, A., Chen, B. H., Assimes, T. L., Bandinelli, S., Hou, L., Baccarelli, A. A., Stewart, J. D., Li, Y., Whitsel, E. A., Wilson, J. G., Reiner, A. P., Aviv, A., Lohman, K., Liu, Y., Ferrucci, L., and Horvath, S. (2018). An epigenetic biomarker of aging for lifespan and healthspan. Aging, 10(4):573–591.

Lewinsohn MA, Bedford T, Müller NF, Feder AF. State-dependent evolutionary models reveal modes of solid tumour growth. Nat Ecol Evol. 2023 Apr;7(4):581-596. doi: 10.1038/s41559-023-02000-4.

Lewitus E, Morlon H. Characterizing and Comparing Phylogenies from their Laplacian Spectrum. Syst Biol. 2016 May;65(3):495-507. doi: 10.1093/sysbio/syv116.

Lodato MA, Rodin RE, Bohrson CL, Coulter ME, Barton AR, Kwon M, Sherman MA, Vitzthum CM, Luquette LJ, Yandava CN, Yang P, Chittenden TW, Hatem NE, Ryu SC, Woodworth MB, Park PJ, Walsh CA. Aging and neurodegeneration are associated with increased mutations in single human neurons. Science. 2018 Feb 2;359(6375):555-559. doi: 10.1126/science.aao4426.

López-Otín C, Blasco MA, Partridge L, Serrano M, Kroemer G. Hallmarks of aging: An expanding universe. Cell. 2023 Jan 19;186(2):243-278. doi: 10.1016/j.cell.2022.11.001.

Macdonald-Dunlop E, Taba N, Klarić L, Frkatović A, Walker R, Hayward C, Esko T, Haley C, Fischer K, Wilson JF, Joshi PK. A catalogue of omics biological ageing clocks reveals substantial commonality and associations with disease risk. Aging (Albany NY). 2022 Jan 24;14(2):623-659. Doi: 10.18632/aging.203847.

Marongiu F, DeGregori J. The sculpting of somatic mutational landscapes by evolutionary forces and their impacts on aging-related disease. Mol Oncol. 2022 Sep;16(18):3238-3258. doi: 10.1002/1878-0261.13275.

Massaar S, Sanders MA. The etiology of clonal mosaicism in human aging and disease. Aging and Cancer. 2023 doi: 10.1002/aac2.12061.

Mitchell E, Spencer Chapman M, Williams N, Dawson KJ, Mende N, Calderbank EF, Jung H, Mitchell T, Coorens THH, Spencer DH, Machado H, Lee-Six H, Davies M, Hayler D, Fabre MA, Mahbubani K, Abascal F, Cagan A, Vassiliou GS, Baxter J, Martincorena I, Stratton MR, Kent DG, Chatterjee K, Parsy KS, Green AR, Nangalia J, Laurenti E, Campbell PJ. Clonal dynamics of haematopoiesis across the human lifespan. Nature. 2022 Jun;606(7913):343-350. doi: 10.1038/s41586-022-04786-y.

Partridge L, Deelen J, Slagboom PE. Facing up to the global challenges of ageing. Nature. 2018 Sep;561(7721):45-56. doi: 10.1038/s41586-018-0457-8.

Pedregosa, F., Varoquaux, G., Gramfort, A., Michel, V., Thirion, B., Grisel, O., Blondel, M., Prettenhofer, P., Weiss, R., Dubourg, V., Vanderplas, J., Passos, A., Cournapeau, D., Brucher, M., Perrot, M., and Duchesnay, E. (2011). Scikit-learn: Machine learning in Python. Journal of Machine Learning Research, 12:2825–2830.

Rutledge, J., Oh, H. & Wyss-Coray, T. Measuring biological age using omics data. Nat Rev Genet 23, 715–727 (2022). https://doi.org/10.1038/s41576-022-00511-7.

Salipante SJ, Horwitz MS. Phylogenetic fate mapping. Proc Natl Acad Sci U S A. 2006 Apr 4;103(14):5448-53. doi: 10.1073/pnas.0601265103.

Sankaran VG, Weissman JS, Zon LI. Cellular barcoding to decipher clonal dynamics in disease. Science. 2022 Oct 14;378(6616):eabm5874. doi: 10.1126/science.abm5874.

Schliep KP. phangorn: phylogenetic analysis in R. Bioinformatics. 2011 Feb 15;27(4):592-3. doi: 10.1093/bioinformatics/btq706.

Sender R, Fuchs S, Milo R. Revised Estimates for the Number of Human and Bacteria Cells in the Body. PLoS Biol. 2016 Aug 19;14(8):e1002533. doi: 10.1371/journal.pbio.1002533.

Shen W, Le S, Li Y, Hu F. SeqKit: A Cross-Platform and Ultrafast Toolkit for FASTA/Q File Manipulation. PLoS One. 2016 Oct 5;11(10):e0163962. doi: 10.1371/journal.pone.0163962.

Stadler T, Pybus OG, Stumpf MPH. Phylodynamics for cell biologists. Science. 2021 Jan 15;371(6526):eaah6266. doi: 10.1126/science.aah6266.

Sulston JE, Horvitz HR. Post-embryonic cell lineages of the nematode, Caenorhabditis elegans. Dev Biol. 1977 Mar;56(1):110-56. doi: 10.1016/0012-1606(77)90158-0. PMID: 838129.

Szilard L. On the nature of the aging process. Proc Natl Acad Sci U S A. 1959 Jan;45(1):30-45. doi: 10.1073/pnas.45.1.30.

Van Rossum, G. and Drake, F. L. (2009). Python 3 Reference Manual. CreateSpace, Scotts Valley, CA.

Varma, S. and Simon, R. (2006). Bias in error estimation when using cross-validation for model selection. BMC Bioinformatics, 7(1):91.

Vijg J, Dong X. Pathogenic Mechanisms of Somatic Mutation and Genome Mosaicism in Aging. Cell. 2020 Jul 9;182(1):12-23. doi: 10.1016/j.cell.2020.06.024.

Wasserstrom A, Frumkin D, Adar R, Itzkovitz S, Stern T, Kaplan S, Shefer G, Shur I, Zangi L, Reizel Y, Harmelin A, Dor Y, Dekel N, Reisner Y, Benayahu D, Tzahor E, Segal E, Shapiro E. Estimating cell depth from somatic mutations. PLoS Comput Biol. 2008 May 9;4(4):e1000058. doi: 10.1371/journal.pcbi.1000058.

Wilson GW, Derouet M, Darling GE, Yeung JC. scSNV: accurate dscRNA-seq SNV co-expression analysis using duplicate tag collapsing. Genome Biol. 2021 May 7;22(1):144. doi: 10.1186/s13059-021-02364-5.

Zou, H. (2006). The adaptive lasso and its oracle properties. Journal of the American Statistical Association, 101(476):1418–1429.

Zou, H. and Hastie, T. (2005). Regularization and variable selection via the elastic net. Journal of the Royal Statistical Society. Series B (Statistical Methodology), 67(2):301–320.

Zou, H. and Zhang, H. H. (2009). On the adaptive elastic-net with a diverging number of parameters. The Annals of Statistics, 37(4):1733 – 1751.

Enclosure No. SZ5

Declaration

I, Attila Csordas, student of the Faculty of Medicine of the University of Szeged, aware of my responsibility of the penal law, declare and certify with my signature that my thesis entitled *Cell Tree Age as a new evolutionary model for representing age-associated somatic mutation burden* is entirely the result of **my own work**. I have faithfully and accurately cited all my sources, including books, journals, handouts, and unpublished manuscripts, as well as any other media, such as the Internet, letters, or significant personal communication.

I understand that

- - literal citing without using quotation marks and marking the references
- - citing the contents of a work without marking the references
- - using the thoughts of somebody else whose work was published, as of our own thoughts

are counted as plagiarism.

I declare that I understood the concept of plagiarism and I acknowledge that my thesis will be rejected in case of plagiarism.

Cambridge, UK, 23/02/2024

Attila Csordas

....

Signature of thesis writer